Design and 3D Printing of Reinforcement Connectors for Mortise and Tenon Joints in Solid Wood Chairs

Chen Wang,[a,b,*] Hanyi Huang,[a] Shanxiang Xu,[a] and Jiahao Yu [b]

To address the loosening of mortise and tenon joints in solid wood chairs caused by prolonged use and wood expansion and contraction, this study proposes a reinforcement method using 3D-printed connectors based on polyethylene terephthalate-1,4-cyclohexanedimethanol (PETG) filament. First, the influence of key process parameters (extrusion extent, nozzle travel speed, and nozzle temperature) on the mechanical properties of PETG models was analyzed. Subsequently, based on the optimized process parameters, reinforcement connectors with rib structures were designed and 3D printed. The reinforcement effectiveness was evaluated by comparing the ultimate load of mortise and tenon joints with and without the reinforcement connectors. Results indicated that with the increase of extrusion extent and nozzle temperature, and the decrease of nozzle travel speed, the ultimate strength and Young's modulus of PETG models increased, improving their mechanical properties. The optimal process parameters were determined as follows: extrusion extent of 105%, nozzle travel speed of 70 mm/s, and nozzle temperature of 250 °C. After installing the reinforcement connectors, the average ultimate load of the mortise and tenon joints reached 445.7 N, which was 34.9% higher than that of joints without reinforcement, demonstrating that the 3D-printed connectors effectively reinforced and protected the mortise and tenon joints.

DOI: 10.15376/biores.21.1.1388-1396

Keywords: Solid wood chair; Mortise and tenon joints; Reinforcement connectors; 3D printing

*Contact information: a: College of Furnishings and Industrial Design, Nanjing Forestry University, Nanjing 210037, China; b: Jiangsu Co-Innovation Center of Efficient Processing and Utilization of Forest Resources, Jiangsu, China; *Corresponding author: 996869559@qq.com*

INTRODUCTION

Chinese solid wood chairs, as furniture embodying traditional culture and practical value, derive their structural charm from mortise and tenon joints. This construction not only lends the furniture an overall aesthetic appeal but also exemplifies the seamless integration of traditional craftsmanship with natural materials (Hu *et al.* 2024). However, the reliability of mortise and tenon joints is highly dependent on the inherent physical properties of the timber itself. As a natural anisotropic material, timber exhibits pronounced hygroscopic properties, absorbing and releasing moisture in response to ambient temperature and humidity fluctuations (Hu *et al.* 2021). This continuous cycle of moisture uptake and desorption readily induces dimensional changes in the timber, consequently affecting the precision of mortise and tenon fits. Over time, under the stress of repeated drying and wetting cycles, the originally tight fit between tenon and mortise gradually loosens (Chen *et al.* 2022). This significantly compromises the chair's structural stability and service life.

The structural weak points of solid wood chairs typically occur at right-angled joint areas, such as the connection between chair legs and horizontal stretchers. These areas are subjected to shear and torsional forces during long-term use, and if relying solely on mortise and tenon joints, they are prone to developing loose fits (Han *et al.* 2022). To address the issue of loosening in mortise and tenon joints, the traditional reinforcement method often involves installing metal corner brackets. While this approach helps restore the structural strength of the mortise and tenon joints to some extent, it also has notable drawbacks (Hang *et al.* 2025). On the one hand, the differing linear expansion coefficients between metal and timber can cause secondary loosening of mortise and tenon joints due to mismatched deformation during temperature fluctuations (Wang *et al.* 2022). On the other hand, conventional metal reinforcement components are often standardised in size, making them ill-suited to accommodate the diverse forms of mortise and tenon joints and varied damage patterns. They lack the bespoke characteristics required for specific mortise and tenon structures (Wang *et al.* 2023).

In recent years, the rapid advancement of 3D printing technology has offered novel solutions to the aforementioned challenges. Leveraging its capabilities for free-form fabrication, rapid prototyping, and personalised customisation; 3D printing can produce connectors that closely match the contours of specific mortise and tenon joints, thereby effectively reinforcing and protecting these joints (Huang *et al.* 2022). Polyethylene terephthalate-1,4-cyclohexanedimethanol (PETG) is a thermoplastic material exhibiting favourable thermoforming properties and chemical resistance. It is economical and environmentally friendly and has a wide range of applications in the field of 3D printing (Li *et al.* 2022). This study selected PETG filament as the raw material. To effectively improve the mechanical properties of 3D-printed PETG models, an analysis was conducted on three critical process parameters (extrusion extent, nozzle travel speed, and nozzle temperature) that significantly influence mechanical properties (Xia *et al.* 2024). Based on the optimized parameters, 3D-printed connectors characterized by low cost, high precision, and excellent mechanical properties were manufactured. This research provides an innovative and practical strategy for reinforcing mortise and tenon joints, ultimately improving the structural stability and service life of solid wood chairs.

EXPERIMENTAL

Materials

The PETG filament (Miracle 3D, Suzhou, China) with a melting point of 220 °C and a density of 1.27 g/cm^3 was employed for 3D printing *via* fused deposition modeling technology.

Specimen Preparation

The tensile ultimate strength and Young's modulus effectively characterise the strength and stiffness of 3D-printed models, serving as key parameters for evaluating their mechanical properties. This study tested the tensile properties of 3D-printed PETG models (Li *et al.* 2023). Following ASTM D638-14 (2022) standard, type I dumbbell-shaped specimens were selected for tests. The specimens were designed using SolidWorks software (Education version, Dassault, Paris, France), with dimensions as shown in Fig. 1.

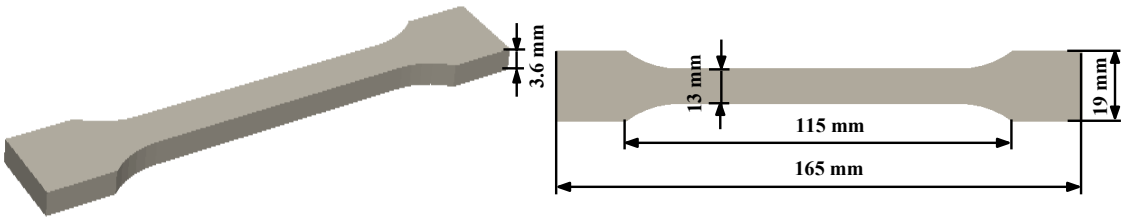

Fig. 1. Tensile test specimen

Dumbbell-shaped specimens were fabricated using PETG filament and a desktop 3D printer (0.4 mm nozzle, Miracle 3D, Suzhou, China), with primary process parameters set as follows: layer height (0.2 mm), infill pattern (grid), infill density (50%), and heated bed temperature (60 °C). All specimens were printed under identical environmental conditions (temperature 23 ± 2 °C, relative humidity 50 ± 5%) to eliminate the influence of environmental factors on the test results.

Performance Test

Following the method specified in ASTM D638-14 (2022), tensile tests were conducted on dumbbell-shaped specimens using a universal testing machine (AG-X, Shimadzu, Kyoto, Japan). The tests were performed under quasi-static loading conditions, applying a constant tensile speed (2 mm/min) to induce axial deformation of the specimens until fracture (Mo *et al.* 2022). By analysing the stress-strain curve during tensile testing, it is possible to evaluate mechanical properties, such as ultimate strength and Young's modulus. The ultimate strength corresponds to the maximum stress value at the peak point of the stress-strain curve, while Young's modulus is calculated by performing a linear regression on the linear segment of the stress-strain curve.

An optical microscope (CL-40M, Colomer; Guangzhou, China) was used to observe the cross-sections of the fractured PETG specimens.

RESULTS AND DISCUSSION

Effect of Extrusion Extent on the Mechanical Properties of PETG Models

Extrusion extent indicates the actual volume of PETG melt extruded from the nozzle per unit time. Mechanical properties of PETG models printed at three extrusion extents (95%, 100%, and 105%) were tested under conditions of 250 °C nozzle temperature and 30 mm/s nozzle travel speed. As evident from Fig. 2, both the ultimate strength and Young's modulus of the PETG models increased with the increase of extrusion extent. The 3D-printed PETG models exhibited a layer-by-layer deposition characteristic (Liu *et al.* 2025). The cross-sectional shape of the PETG melt extruded from the nozzle was approximately elliptical, readily forming voids at the bonding interface with adjacent melt (Qi *et al.* 2023). However, as the extrusion extent increased, the volume of melt extruded from the nozzle per unit time increased. Under the force of extrusion, the melt underwent flow and spreading at the bonding interface, thereby filling the voids (reducing voids' volume, as shown in Fig. 3) and improving the interfacial bonding properties of the melt (Liu *et al.* 2021). Consequently, increasing extrusion extent can effectively improve the mechanical properties of PETG models.

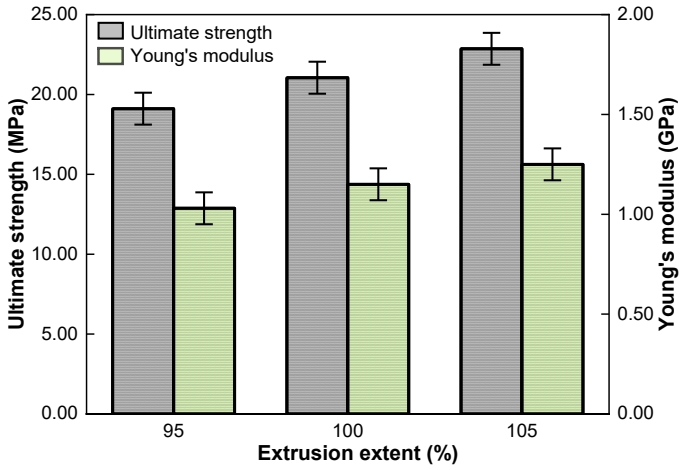

Fig. 2. Effect of extrusion extent on the mechanical properties of PETG models

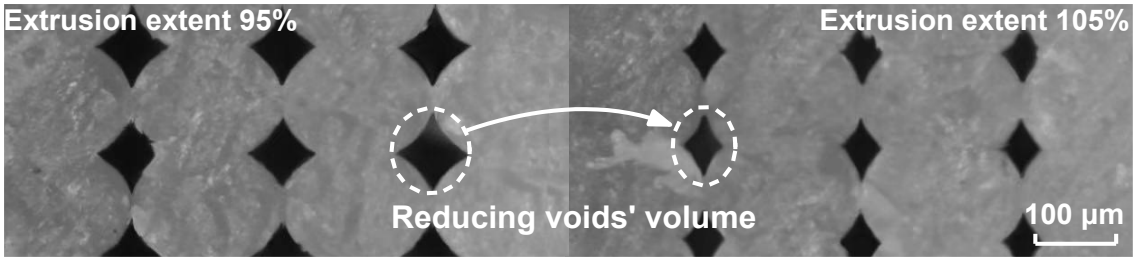

Fig. 3. Detailed magnified image

Effect of Nozzle Travel Speed on the Mechanical Properties of PETG Models

Nozzle travel speed refers to the velocity of a 3D printer nozzle traversing the X-Y plane during model contour filling. Mechanical properties of PETG models printed at three nozzle travel speeds (30, 50, 70 mm/s) were tested under conditions of 250 °C nozzle temperature and 105% extrusion extent. As evident from Fig. 4, both the ultimate strength and Young's modulus of the PETG models increased with the decrease of nozzle travel speed.

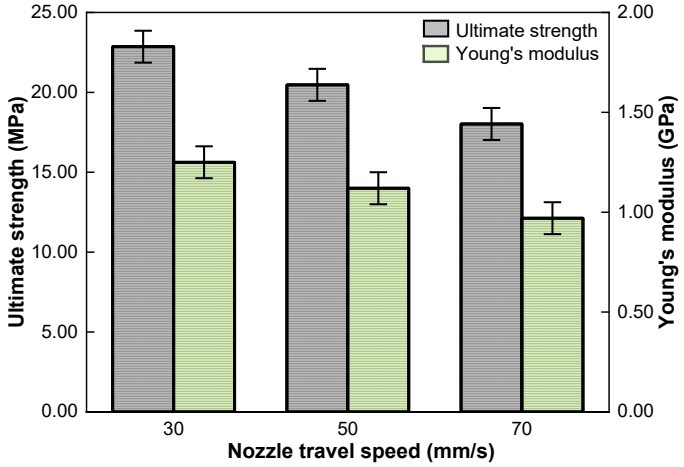

Fig. 4. Effect of nozzle travel speed on the mechanical properties of PETG models

This occurs because when the nozzle travel speed increases, the extrusion volume of the PETG melt becomes relatively insufficient. Consequently, the cross-sectional width of the melt extruded from the nozzle diminishes, leading to the formation of voids between the adjacent melt (Yang *et al.* 2022). Furthermore, increased nozzle travel speed intensifies vibrations within the FDM printer, compromising print accuracy and increasing internal voids within the model. These voids act as structural weak points, readily inducing stress concentration under load and consequently leading to model failure (Yu *et al.* 2024). Consequently, reducing nozzle travel speed can effectively improve the mechanical properties of PETG models.

Effect of Nozzle Temperature on the Mechanical Properties of PETG Models

Mechanical properties of PETG models printed at three nozzle temperatures (230, 240, and 250 °C) were tested under conditions of a 30 mm/s nozzle travel speed and 105% extrusion extent. As evident from Fig. 5, both the ultimate strength and Young's modulus of the PETG models increased with the increase of nozzle temperature. This is because the elevated nozzle temperature raises the temperature of the PETG melt, reducing its viscosity and enhancing its flowability (Yu *et al.* 2023). This facilitates better spreading of the melt at the bonding interface. Furthermore, elevated nozzle temperatures accelerate molecular motion within the PETG melt at the bonding interface (Zhang *et al.* 2025). This promotes diffusion and entanglement between adjacent melt chains, enhancing interfacial adhesion properties (Zhu *et al.* 2024). Consequently, increasing nozzle temperature can effectively improve the mechanical properties of PETG models.

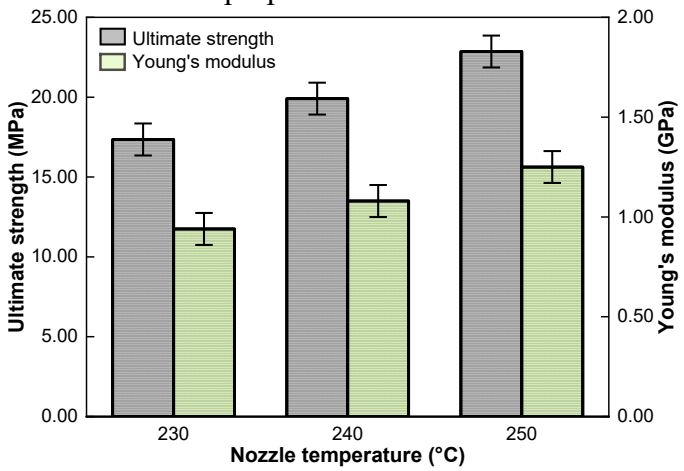

Fig. 5. Effect of nozzle temperature on the mechanical properties of PETG models

3D Printing

This study took the T-shaped mortise and tenon joint of a solid wood chair as an example to design and 3D print reinforcement connector. First, the dimensions of the T-shaped mortise and tenon joint were measured, and a 3D model of the joint was constructed using SolidWorks software. Subsequently, the 3D model of the reinforcement connector was generated using the equal thickness offset function, with an offset thickness of 1.0 mm. To further enhance the reinforcement effect of the connector, triangular ribs were added to the right-angled areas of the connector, drawing inspiration from the rib structures commonly used in injection-moulded parts. This structure effectively mitigates damage to the mortise and tenon joint caused by shear and torsional forces. The final 3D model of the reinforcement connector is shown in Fig. 6a.

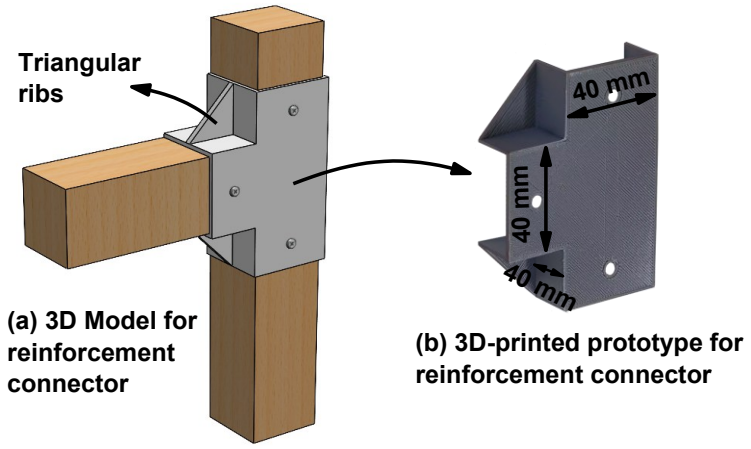

Fig. 6. 3D model and 3D-printed prototype of reinforcement connector

To effectively improve the mechanical properties of the reinforcement connector, the optimal process parameters obtained from the aforementioned tests were applied: the extrusion extent was set to 105%, the nozzle temperature to 250 °C, and the nozzle travel speed to 30 mm/s. Furthermore, to balance factors, such as material cost and printing time for the connector, the conventional process parameters were set as follows: Layer height (0.2 mm), infill pattern (grid), infill density (50%), and heated bed temperature (60 °C). Subsequently, the processing data was imported into the 3D printer. Once the nozzle and heated bed had completed preheating, 3D printing commenced. The reinforcement connector required 25 min to print, consuming 30 g of PETG filament. The final printed reinforcement connector is shown in Fig. 6b. This 3D-printed connector combined low cost, high precision, and excellent mechanical properties. It was installed onto the mortise and tenon joint using self-tapping screws, thereby achieving reinforcement of the joint.

Comparative Test

Comparative flexural strength tests were conducted on T-shaped mortise and tenon joints with and without connectors (Fig. 7).

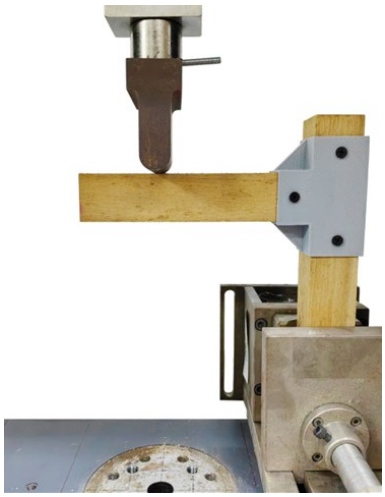

Fig. 7. Comparative test apparatus

Test specimens were manufactured from identical timber, dimensions, and equipment, comprising poplar wood with an air-dry density of 0.4 g/cm³ and a moisture content of 10%. The specimens employed rectangular tenon joints (length: 25 mm, width: 15 mm, thickness: 20 mm), with both tenons and mortises machined on a CNC lathe to a precision of 0.01 mm. The rectangular tenon joint fit parameters were as follows: an interference fit in the tenon width direction with a clearance of 0.1 mm; a clearance fit in the tenon thickness direction with a clearance of 0.1 mm; and a clearance fit in the tenon length direction with a clearance of 1.0 mm.

The comparative tests were conducted across 10 groups, with 5 groups fitted with reinforcement connectors and 5 groups without. The comparative test apparatus is illustrated in Fig. 7. Flexural tests were performed on a universal testing machine at a loading rate of 10 mm/min. The ultimate load value was recorded for each group, with results presented in Fig. 8. As evident from Fig. 8, the average ultimate load for mortise and tenon joints fitted with reinforcement connectors reached 445.7 N. This represented a 34.9% increase compared to joints without reinforcement connectors (average ultimate load: 330.2 N). This demonstrates that the 3D-printed connectors effectively reinforced and protected mortise and tenon joints.

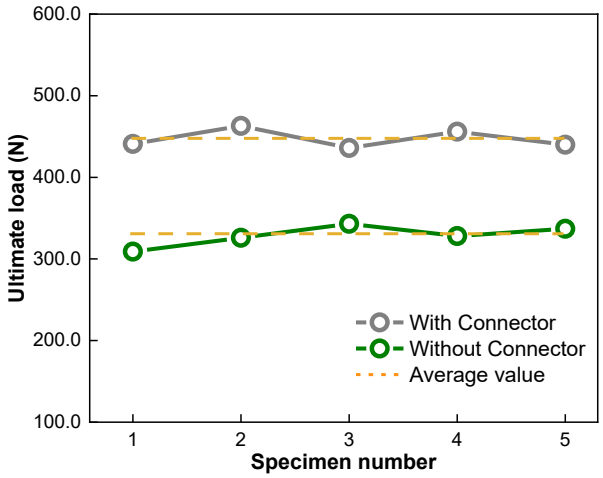

Fig. 8. Bending resistance test of mortise and tenon joints

CONCLUSIONS

1. This study analysed the influence of key process parameters (extrusion extent, nozzle travel speed, and nozzle temperature) on the mechanical properties of polyethylene terephthalate-1,4-cyclohexanedimethanol (PETG) prototypes. Experimental results indicate that with the increase of extrusion extent and nozzle temperature, and the decrease of nozzle travel speed, the ultimate strength and Young's modulus of PETG models increase, enhancing their mechanical properties. The optimal process parameters were determined as follows: extrusion extent of 105%, nozzle travel speed of 70 mm/s, and nozzle temperature of 250 °C.
2. Using PETG filament as the raw material, a reinforced connector featuring rib structures was designed and 3D-printed based on optimized process parameters. This connector showed characteristics including low cost, high precision, and excellent

mechanical properties. Following installation of the reinforced connector, the average ultimate load capacity of the mortise and tenon joints increased 34.9%, demonstrating that the connector effectively achieves reinforcement and protection of these joints.

REFERENCES CITED

ASTM D638-14 (2022). "Standard test method for tensile properties of plastics," ASTM International, West Conshohocken, PA, USA.

Chen, B.-R., Yu, X.-J., and Hu, W.-G. (2022). "Experimental and numerical studies on the cantilevered leg joint and its reinforced version commonly used in modern wood furniture," *BioResources* 17(3), 3952-3964. https://doi.org/10.15376/biores.17.3.3952-3964

Han, Y., Yan, X.-X., and Zhao, W.-T. (2022). "Effect of thermochromic and photochromic microcapsules on the surface coating properties for metal substrates," *Coatings* 12(11), article 1642. https://doi.org/10.3390/coatings12111642

Hang, J.-Y., Zou, Y.-M., Yan, X.-X., and Li, J. (2025). "Preparation of thermochromic UV coating with urea-formaldehyde-coated ternary system on bleached poplar wood surface," *Coatings* 15(9), article 997. https://doi.org/10.3390/coatings15090997

Hu, W.-G., Li, S., and Liu, Y. (2021). "Vibrational characteristics of four wood species commonly used in wood products," *BioResources* 16(4), 7101-7111. https://doi.org/10.15376/biores.16.4.7101-7111

Hu, W.-G., Zhao, Y., Xu, W., and Liu, Y.-Q. (2024). "The influences of selected factors on bending moment capacity of case furniture joints," *Applied Sciences* 14(21), article 10044. https://doi.org/10.3390/app142110044

Huang, N., Yan, X.-X., and Zhao, W.-T. (2022). "Influence of photochromic microcapsules on properties of waterborne coating on wood and metal substrates," *Coatings* 12(11), article 1750. https://doi.org/10.3390/coatings12111750

Li, S., and Hu, W.-G. (2023). "Study on mechanical strength of cantilever handrail joints for chair," *BioResources* 18(1), 209-219. https://doi.org/10.15376/biores.18.1.209-219

Li, W.-B., Yan, X.-X., and Zhao, W.-T. (2022). "Preparation of crystal violet lactone complex and its effect on discoloration of metal surface coating," *Polymers* 14(20), article 4443. https://doi.org/10.3390/polym14204443

Liu, Q., Gu, Y., Xu, W., Lu, T., Li, W., and Fan, H. (2021). "Compressive properties of green velvet material used in mattress bedding," *Applied Sciences* 11(23), article 11159. https://doi.org/10.3390/app112311159

Liu, Y., Li, J.-Y., and Hu, W.-G. (2025). "Aesthetic preferences of Minnan folk wooden altar table," *BioResources* 20(4), 10425-10446. https://doi.org/10.15376/biores.20.4.10425-10446

Mo, X.-F., Zhang, X.-H., Fang, L., and Zhang, Y. (2022). "Research progress of wood-based panels made of thermoplastics as wood adhesives," *Polymers* 14(1), article 98. https://doi.org/10.3390/polym14010098

Qi, Y.-Q., Sun, Y., Zhou, Z.-W., Huang, Y., Li, J.-X, and Liu, G.-Y. (2023). "Response surface optimization based on freeze-thaw cycle pretreatment of poplar wood dyeing effect," *Wood Research* 68(2), 293-305. https://doi.org/10.37763/wr.1336-4561/68.2.293305

Wang, L., Han, Y., and Yan, X.-X. (2022). "Effects of adding methods of fluorane microcapsules and shellac resin microcapsules on the preparation and properties of bifunctional waterborne coatings for basswood," *Polymers* 14(18), article 3919. https://doi.org/10.3390/polym14183919

Wang, Q., Feng, X.-H., and Liu, X.-Y. (2023). "Functionalization of nanocellulose using atom transfer radical polymerization and applications: A review," *Cellulose* 30, 8495-8537. https://doi.org/10.1007/s10570-023-05403-5

Xia, F., Wang, W., Zhang, J.-H., Yang, Y.-T., Wang, Q.-Y., and Liu, X.-Y. (2024). "Improving weed control through the synergy of waste wood-based panels pyrolysis liquid and rice husks: A sustainable strategy," *BioResources* 19(4), 7606-7618. https://doi.org/10.15376/biores.19.4.7606-7618

Yang, Z.-Z., Feng, X.-H., Xu, M., and Rodrigue, D. (2022). "Printability and properties of 3D printed poplar fiber/polylactic acid biocomposites," *BioResources* 16(2), 2774-2788. https://doi.org/10.15376/biores.16.2.2774-2788

Yu, S.-L., Zheng, Q., Chen, T.-Y., Zhang, H.-L., and Chen, X.-R. (2023). "Consumer personality traits vs. their preferences for the characteristics of wood furniture products," *BioResources* 18(4), 7443-7459. https://doi.org/10.15376/biores.18.4.7443-7459

Yu, S.-L., and Wu, Z.-H. (2024). "Research on the influence mechanism of short video communication effect of furniture brand: Based on ELM model and regression analysis," *BioResources* 19(2), 3191-3207. https://doi.org/10.15376/biores.19.2.3191-3207

Zhang, W.-J., Zou, Y.-M., Yan, X.-X., and Li, J. (2025). "Influence of two types of microcapsule composites on the performance of thermochromic UV coatings on bleached poplar wood surfaces," *Coatings* 15(9), article 1001. https://doi.org/10.3390/coatings15091001

Zhu, Y., Wang, Y., and Yan, X.-X. (2024). "Preparation of chitosan-coated *Toddalia asiatica* (L.) lam extract microcapsules and its effect on coating antibacterial properties," *Coatings* 14(8), article 942. https://doi.org/10.3390/coatings14080942

Article submitted: November 25, 2025; Peer review completed: December 17, 2025; Revised version received and accepted: December 22, 2025; Published: December 26, 2025.
DOI: 10.15376/biores.21.1.1388-1396